Sensors & Actuators: B. Chemical 446 (2026) 138689

Contents lists available at ScienceDirect

Sensors and Actuators: B. Chemical

journal homepage: www.elsevier.com/locate/snb

On-chip electrochemical detection of dissolved oxygen: Eliminating the requirement for a permeable selective membrane

Ian Seymour, Fiona Barry, Alan O'Riordan, James F. Rohan *

Tyndall National Institute, Lee Maltings, University College Cork, Cork T12 R5CP, Ireland

ARTICLE INFO

Keywords:
Microfabricated
Dissolved oxygen
Sensor
Hydrogen peroxide
Interdigitated array
Dual-metal
Generator-collector

ABSTRACT

Membrane-free electrochemical dissolved oxygen sensors were developed using micro interdigitated electrode arrays. The optimised sensor for detection of dissolved oxygen should contain a gold generator electrode to produce hydrogen peroxide, and a platinum collector electrode for the subsequent detection. The microfabrication process required platinum electrodeposition onto one comb of a gold interdigitated array. The deposition also decreased the inter-electrode gap and increased the collection efficiency. The dual metal IDE was then used to sense dissolved oxygen in water. A pre-treatment step was also required to improve the sensitivity of platinum to hydrogen peroxide ensuring a clean, reproducible surface for each test. The developed sensor accurately detected oxygen concentrations between 0 and 9 ppm, with a sensitivity of 1.59 nA/ppm and an LOD of 0.36 ppm. The detection of oxygen was also tested in the presence of unknown interferents, in estuarine river water, and with known interferents. It was found that the magnitude of hydrogen peroxide oxidation was generally unaffected by the presence of interferents, indicating a potential for interferent free oxygen detection without the requirement of oxygen permeable membranes.

1. Introduction

Dissolved oxygen (DO) refers to the amount of gaseous oxygen that a water system contains. DO arises primarily from two main processes: photosynthesis and diffusion from the atmosphere. Agitated water systems will dissolve more oxygen through diffusion, therefore flowing and tidal water systems are expected to have higher DO concentrations than stagnant or quiescent waters[1]. Temperature, salinity, and altitude are just some of the natural environmental factors that can influence the DO concentration. Dramatic and unexpected decreases in DO concentration typically result from contamination of the water source. The most common contaminants are bacteria and organic matter. Nutrient run-off from fertilizers is also a major source of contamination that can dramatically reduce DO in water[2]. From this, it is evident that DO can be an indicator of the overall health of the water system. A decrease in DO or the presence of pollutants becomes apparent quickly in river and lake waters, due to eutrophication. For potable water, however, this is not as readily apparent. Therefore, it is necessary to actively monitor drinking water systems to ensure that the water is safe to consume. Regular monitoring of DO in drinking water can establish a baseline of normal or healthy conditions[3]. Significant deviations from this normal condition can therefore indicate an issue, most likely due to contamination.

Current approaches to DO sensing are based on optical or electrochemical detection mechanisms, both of which can be undertaken at the point-of-interest. Optical based DO sensors typically operate by measurement of the luminescence response of a molecule in the presence of oxygen, where higher concentrations of oxygen mean less luminescence, leading to a quantitative measurement[4]. The luminescent species, typically an organic molecule, is provided as part of the overall device, simplifying the analysis. A drawback, however, is that luminescent species need to be replenished over time and can be influenced by environmental factors, such as temperature, pH and self-quenching. Electrochemical approaches to DO sensing, typically involve measurement by direct reduction of oxygen at an electrode surface. The reaction that governs this is shown in Eq. 1[5,6].

$$O_2 + \quad 4H^+ + \quad 4e^- \rightarrow \quad 2H_2O \tag{1}$$

However, the oxygen reduction reaction is subject to interference from other species, particularly in a complex matrix like water. It can also complicate the electrochemical detection of other species in water due to the large reaction potential window[7]. To this end,

* Corresponding author.
E-mail address: james.rohan@tyndall.ie (J.F. Rohan).

https://doi.org/10.1016/j.snb.2025.138689
Received 26 June 2025; Received in revised form 19 August 2025; Accepted 2 September 2025
Available online 3 September 2025

electrochemical approaches therefore require an oxygen permeable membrane behind which, the electrodes and electrolyte are placed. The membrane acts to ensure that only oxygen reaches the electrode surface by blocking other ions[8]. While this approach is less expensive than the optical method, issues arise when trying to miniaturise the sensor device due to the requirement for a membrane. Miniaturisation is important to facilitate portability, but also to minimise consumption of oxygen. Reduction of oxygen is a destructive process, as the oxygen is irreversibly reduced to water, therefore, larger electrodes may inadvertently deplete the DO concentration with consequent false negatives. However, complex fabrication methods are required for membrane integration at smaller length scales, and as a result much research focuses on improving these methods[9–11]. While elimination of the membrane would facilitate the miniaturisation of devices, it could also lead to interferents, such as chlorine, adversely affecting the DO detection. In this work, we propose a method to quantify DO using interdigitated electrode arrays (IDE) without the need for a membrane while also eliminating common interferent effects. In this approach, hydrogen peroxide, produced as an intermediate species in oxygen reduction, is used as an indicator of overall DO concentration. This pathway is shown by Eq. 2 and Eq. 3 [12,13]

$$O_2 + \quad 2H^+ + \quad 2e^- \quad \rightleftharpoons \quad H_2O_2 \tag{2}$$

$$H_2O_2 + \quad 2H^+ + \quad 2e^- \quad \rightleftharpoons \quad 2H_2O \tag{3}$$

Eqs. 1 – 3 effectively show a simplified mechanism for the oxygen reduction reaction. A more detailed discussion of this reaction is included in the supplementary information (SEq. 1 – 13). This method permits facile, interference-free DO quantification, without the need for an oxygen permeable membrane, consequently enabling miniaturisation. The detection of hydrogen peroxide during oxygen reduction has classically been achieved using a rotating ring disc electrode (RRDE) configuration[14–16]. in that method, hydrogen peroxide produced at the disc moves to the outer ring electrode by convection forces, for detection. Typically, the collection efficiencies are quite low by comparison with generator-collector experiments which utilise a redox couple[17]. Collection efficiencies of 15–25 % are considered high for the RRDE with quite complex instrumentation which is unsuitable for miniaturised or portable sensing applications. An alternative to the RRDE for the detection of produced hydrogen peroxide is the use of IDEs. In this approach, detection is governed by diffusion of hydrogen peroxide from the generator to the collector rather than convection. This has been shown to be a viable approach by Postlethwaite et al., using IDEs with 10 μm width and 10 μm gaps[18]. A drawback of this approach at the dimensions investigated was a lower collection efficiency of 5 % by comparison to the RRDE approaches.

IDEs with smaller interelectrode gaps, such as 1 μm, would be expected to increase the efficiency significantly in line with ring-disc approaches. In the RRDE set-up, at the ring collector electrode the product of oxidised hydrogen peroxide (i.e., oxygen) is removed to the bulk electrolyte by the prevailing convection forces. In the IDE set-up, the product can diffuse back to the generator electrode to be reduced again, thus improving sensitivity. This IDE approach permits redox cycling, i.e., where the same molecule can be reduced and oxidised repeatedly or the control of the local environment, such as local pH control, by imposition of an appropriate potential at the collector electrode to enable novel analysis that is not otherwise possible [19,20].

In this work, we extended the previous research with IDE and local environment control to investigate the detection of oxygen through its electrochemical reduction to hydrogen peroxide at the generator electrode subsequently detected by oxidation of the peroxide at the collector electrode. Binary Gold and platinum IDEs were investigated to determine which material performs better at this scale. Fabrication of single metal IDEs requires fewer processing steps than a mixed metal binary IDE, therefore sensor devices comprising two IDEs were fabricated as either gold-gold or platinum-platinum. While gold was anticipated to be the superior metal in reducing DO via the two-electron reduction to hydrogen peroxide, platinum was also explored as it may have the appropriate behaviour at the ultra-micro scale to suit the desired detection method. The ability of both gold and platinum to oxidise hydrogen peroxide was also investigated to establish the preferred collector material. Parameters were established for the appropriate sensing technique, including the relevant pre-treatment steps. Finally, the method was applied to detection of DO in estuarine river water samples and those containing common reductive interferents to establish the viability of the sensor in real world applications.

2. Materials and methods

2.1. Device fabrication and characterization

Silicon chip-based devices were fabricated using methods similar to those described by Creedon et al. and Barry et al[21,22]. Each chip consisted of two combs of gold working IDEs. A platinum pseudo reference and gold counter electrode were also employed on-chip. In brief, chips were designed to interface with external electronics via a microSD port to facilitate facile electrical connection. Devices were batch fabricated on 4-inch silicon wafers with a 300 nm thermally grown silicon dioxide insulation layer. Blanket deposits of titanium (10 nm) and gold (100 nm) was undertaken using a Temescal FC-2000 E-beam evaporator and lift-off technique to yield interdigitated microband (Length 55 μm x Width 1 μm x Height 110 nm) structures with separations between the tines of each comb maintained at 1.2 μm. A second metal evaporation and lift-off process was undertaken to define the interconnection tracks, contact pads and the gold counter electrode (90 μm x 7 mm). To prevent unwanted interactions along the connection tracks an insulating layer of silicon nitride was deposited by plasma enhanced chemical vapor deposition. Photolithography and dry etching were utilized to selectively open windows (45 μm x 100 μm) in the insulating nitride layer over the microband electrodes for electrolyte access. Openings were also created over the counter and reference electrodes and the contact pads. Each chip contains six IDE (sensors) which are separated by 0.94 mm to prevent cross talk between the sensors. Once sensor fabrication was completed, each wafer was diced to yield 28 separate chips.

A typical micrograph of one such chip is shown in Fig. 1(a), with the sensor array shown in Fig. 1(b). A custom-made cell holder was fabricated to allow measurement with small electrolyte volumes (~50 μL to 5 mL.). The cell was constructed from an aluminium base and a Teflon lid. Spring loaded probes (Coda Systems Ltd. PM4J Plain Radius Microprobes) were inserted into the lid in position above the peripheral contact pads, to permit electrical connection to external potentiostats. The cell was assembled with a Viton O-ring embedded in the lid to form a seal around the on-chip electrodes. Viton O-rings were chosen for their chemical resistance. The inner diameter of the O-ring was 7 mm with a cross section of 1.6 mm to allow an opening large enough for an electrolyte volume of 5 mls to expose all six sensors, counter, and reference electrodes on the device. Each chip was inspected using optical microscopy to identify any obvious defects or faults. Prior to any electrochemical characterisation chips were cleaned by rinsing for 20 s with acetone, iso-propyl alcohol and finally de-ionized water. The chips were dried in a flow of nitrogen and placed in the chip holder.

Electrochemical analysis was performed using an Autolab Bipotentiostat (MAC80150 with BA Module, Metrohm). Cyclic voltammograms (CV) were performed from 0 V to 0.6 V at 50 mV/s in 1 mM ferrocene carboxylic acid (FCA, Sigma Aldrich, 97 %) dissolved in 10 mM phosphate buffered saline (PBS, Sigma Aldrich). During these scans, the second interdigitated comb of electrodes was held at 0 V. All electrochemical measurements were recorded versus a commercial Ag/AgCl. Optical micrographs were acquired using a calibrated microscope (Axioskop II, Carl Zeiss Ltd.) with a charge-coupled detector camera (CCD; DEI-750, Optronics). SEM images were obtained using a

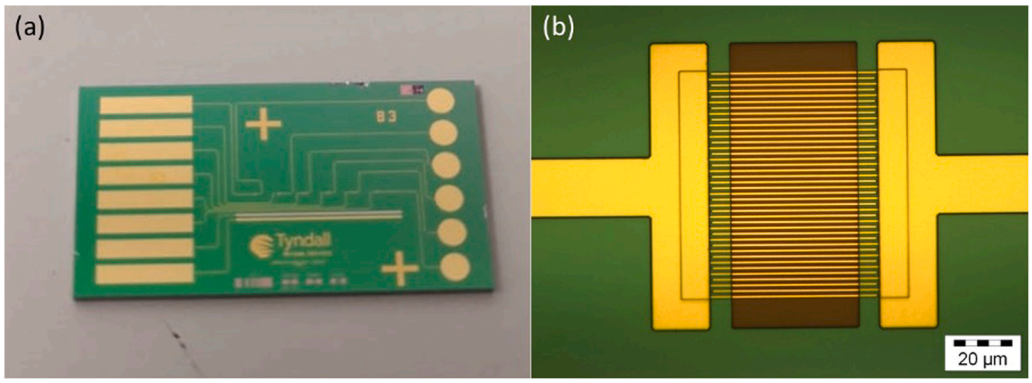

Fig. 1. (a) Fully fabricated silicon chip showing six sensor arrays and on chip counter and reference. (b) Microscope image of one interdigitated sensor array showing two combs of electrodes with each finger 0.8 µm width separated by a 1.2 µm gap.

calibrated field emission FEI Quanta FEG 650 at a beam voltage of 10 kV.

2.2. Electrochemical analysis of DO and hydrogen peroxide on gold and platinum

Electrochemical oxygen reduction was carried out in artificial drinking water (ADW) prepared by dissolving 1 g of sodium bicarbonate, 0.0654 g of magnesium sulphate (Sigma Aldrich, 99.5 % anhydrous), 0.3414 g calcium sulphate dehydrate (Honeywell, 99 %), 0.007 g potassium phosphate dibasic (Fluka, 98 %), potassium phosphate monobasic (Sigma Aldrich, 99 %) and 0.01 g sodium nitrate (Sigma Aldrich, 99 %) in 10 L of deionised water. ADW was allowed to saturate with oxygen by exposure to air at room temperature (~17 °C). All oxygen concentrations were measured using a commercial optical DO probe (Hach, LDO101). Both gold-gold and platinum-platinum IDE arrays were used for this work. CVs were performed in each concentration of oxygen sweeping from 1.2 V to – 0.8 V vs. Ag/AgCl at 50 mV/s for 3 cycles. Varying concentrations of hydrogen peroxide solutions (between 20 and 1000 µM) were prepared by diluting a hydrogen peroxide stock (Sigma Aldrich, 30 % w/w) in ADW. LSVs were performed in each sample in the voltage range of 0.8 V to −0.2 V vs. Ag/AgCl at 50 mV/s. Scans were performed in triplicate for each concentration.

2.3. Optimization of parameters for detection of intermediate hydrogen peroxide from O_2 reduction

ADW samples saturated with oxygen were used to determine which metal, gold or platinum, produced higher quantities of hydrogen peroxide. Both metals can sufficiently oxidise hydrogen peroxide, therefore gold-gold and platinum-platinum generator - collector arrays were used for this analysis. CV analysis using the same parameters described in the previous section was undertaken. The only adjustment made being the biasing of the collector electrode comb at 0.4 V vs. Ag/AgCl.

2.4. Platinum plating on collector electrode comb to form a binary IDE array

Platinum was plated on one comb of a gold IDE to produce gold-platinum arrays with a view to improve the sensitivity of the hydrogen peroxide detection. Platinum was plated using a commercial DNS bath (Johnson Matthey). The collector comb was held at a cathodic current of 0.108 µA for one minute to achieve a platinum plate approximately 83 nm thick.

2.5. Calibration of DO using gold-platinum generator-collector approach

Samples of ADW with varying concentrations of oxygen were prepared by purging ADW solutions with nitrogen for 30 min. After purging, the ADW samples were covered with parafilm which contained a small perforation. This allowed oxygen to partition back into solution, albeit at a slow rate. It was found that oxygen typically re-dissolved at a rate of approximately 1 ppm per 3 min when the concentration was between 0 and 4 ppm. After 4 ppm was reached, the rate slowed to 1 ppm per 7 min until a 6 ppm concentration was reached. To bring the solution back to saturated concentrations, oxygen had to be bubbled into the solution, as the time to reach saturation by diffusion was considerably longer. This resulted in ADW solutions with oxygen concentration varied between fully nitrogen purged (~0.5 ppm), and fully saturated (~8.8 ppm). All oxygen concentrations were first measured using a commercial optical DO probe (Hach, LDO101). CV was performed for each concentration, using the gold-platinum mixed metal IDE, in the voltage window of 1.2 V to −0.8 V vs. Ag/AgCl. The gold generator was scanned while the platinum collector was biased at 0.4 V to oxidise the generated hydrogen peroxide. Prior to any scan, the platinum collector was biased at −0.8 V for 20 s as a pre-treatment step to remove any oxide that may have formed on the surface of the electrode. An alternative approach to construct the analytical curve is the chemical depletion of DO using a standardized bisulfite solution. In this method, the solution is first saturated with oxygen, and then aliquots of bisulfite are added. The resulting decrease in DO concentration is monitored with a calibrated electrode to construct the analytical curve. Nitrogen purging was utilised in this work to minimise any potential addition of further contamination, cross-reactions or potential interferents in the chosen potential window while undertaking highly sensitive generator collector electrochemistry.

2.6. Detection of DO in the presence of known and unknown interferents

Samples of ADW were spiked with 1 mg/L iron ($FeCl_3$, Sigma Aldrich) and 1 mg/L chlorine (NaOCl, Milton Sterilizing Fluid), both of which are known to be active interferents in the oxygen reduction window. The method described above was used to test these samples to determine how both the generator and collector electrodes would be affected by the presence of additional reacting species. Furthermore, samples of river water (taken from River Lee, Cork city) were tested using the same approach. The spiked samples were measured versus a blank ADW sample with an equivalent concentration of DO, as measured by the optical DO probe. Similarly, the river water was tested versus a sample of ADW with equivalent concentrations of DO at the same temperature.

3. Results and discussion

3.1. Characterization of O_2 reduction and hydrogen peroxide oxidation on gold and platinum

Fig. 2(a) shows a comparison of oxygen reduction at gold and platinum electrodes. Both electrodes were immersed in ADW with equivalent concentrations of DO. Oxygen reduction occurred at less negative potentials on platinum, however this reduction proceeds via the one step, four electron pathway to water. The gold electrode reduced oxygen at more cathodic potentials but does so via the two-step pathway. A full explanation of the oxygen reduction reaction is given in the supporting information (SI Eq. 1 – SI Eq. 13). CVs and Calibration plots of DO for both gold and platinum are also presented in supporting information (SI Fig. 1 (a) – (d)) and exhibit sensitivities of 3.2 nA/ppm and 3.8 nA/ppm, respectively. The current measured on the reverse sweep, 30 nA, at the platinum electrode, after the platinum oxide has been reduced, is equivalent to the current measured on gold after the second reduction step. By not allowing the platinum oxide to form, this peak behavior is removed, highlighting that it is solely attributed to the oxide reduction (SI Fig. 2). Both IDEs have the same dimensions, so it was expected that the measured currents should be similar. Diffusional overlap was also observed to be occurring such that the IDE electrodes were acting as one large electrode as opposed to an array of independent microelectrodes.

As the detection method of this sensor involved the oxidation of hydrogen peroxide generated by the reduction of DO, both gold and platinum were evaluated as potential detection materials by comparing their LSV responses in 200 μM hydrogen peroxide. Fig. 2(b) shows the oxidation of hydrogen peroxide on one comb of both a gold IDE and a platinum IDE, respectively. The platinum electrode showed a superior oxidation, with a current taken at 0.7 V that was 1.5 times higher than the gold electrode. An oxidation event was seen at 0.2 V on platinum that was absent for gold. This has been attributed to dissociative binding of hydrogen peroxide to the platinum surface, before its subsequent oxidation and released as oxygen. A full calibration of hydrogen peroxide on platinum is shown in the supporting information (SI Fig. 3 (a) and (b). The appropriate potential for collector electrode biasing was determined from these LSVs. The main peak was observed at 0.65 V for both materials. However, the platinum electrode could be biased at any potential from 0.2 V to 0.7 V and activity would be seen for hydrogen peroxide, which is another advantage over gold. The oxidation event on both materials displayed a peak shaped behaviour. Again, this can be explained by diffusional overlap.

3.2. Generator-collector detection of hydrogen peroxide intermediate

While gold had been established as the better material to differentiate the two-step reduction of oxygen, it was necessary to confirm that detectable amounts of hydrogen peroxide were being produced. This was undertaken using a gold IDE where one comb underwent CV from 1.2 V to −1 V (generator) while the other was biased at a constant potential at 0.6 V (collector), suitable for oxidising hydrogen peroxide. Experiments were performed at 50 mV/s to ensure that the produced hydrogen peroxide could diffuse to the collector before being further reduced at the generator. Fig. 3(a) shows the result of this test performed in oxygen saturated ADW. The generator electrode delivered a current of 31.95 nA, while the collector detected a current of 11.82 nA. From this, a collection efficiency of 44 % was established, which is significantly higher than previous reports for IDEs and ring-disc systems. While this collection efficiency may appear low by comparison with ferrocene-based couples (~95 %), given the complex reaction mechanism associated with oxygen reduction, this is a very high for hydrogen peroxide analysis. Full conversion from oxygen to hydrogen peroxide may not occur, but it is also possible that the subsequent reaction consuming the hydrogen peroxide may result in lower amounts of the species reacting at the detector. This is also why the collector scan shows a peak rather than a steady-state response, as the concentration of hydrogen peroxide is subsequently decreasing. Similarly, the reactions of the two individual species must be considered. In this case, the oxygen is being chemically altered, therefore a simple calculation for collection efficiency is not readily applied.

Significant redox cycling was observed, as evident by the change in overall shape of the CV. The first step of the oxygen reduction current is amplified, by redox cycling between the generator and collector of the oxygen/hydrogen peroxide redox couple. The total current remains the same however, as the second step in the oxygen reduction reaction cannot be redox cycled. A comparison of single mode and generator-collector mode for gold is shown in the supporting Information (SI Fig. 4). The same test was performed on a platinum IDE to further confirm that hydrogen peroxide is not produced in greater quantities. Fig. 3(b) shows that the collector response for platinum under the same conditions is extremely small. The reverse sweep of the generator electrode measured 29 nA, while the collector sweep measured approximately 1.2 nA. Again, the collector efficiency cannot be directly applied but for platinum it is only ~4 %, which is significantly less than the gold electrode. Interestingly, the small amount of hydrogen peroxide produced is only measured on the forward sweep. On gold, hydrogen

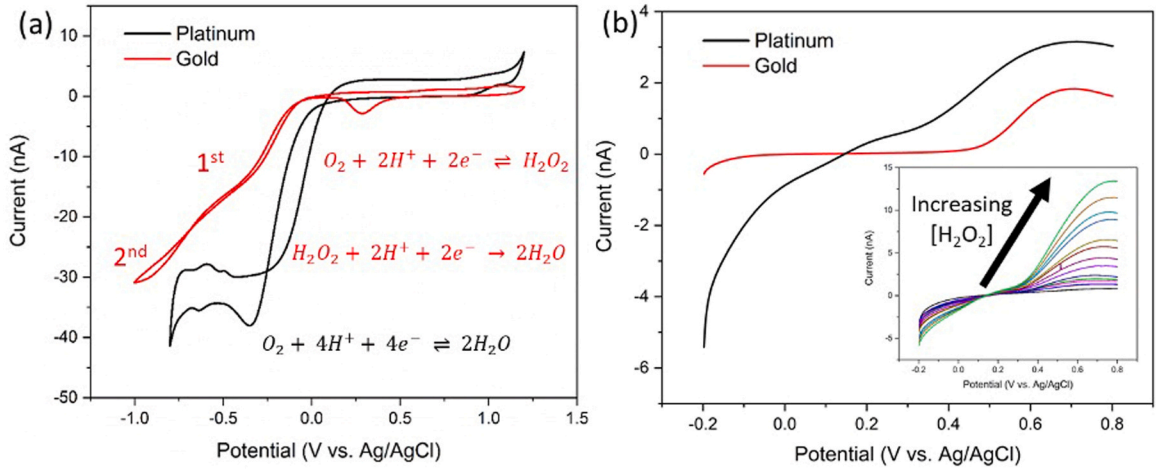

Fig. 2. (a) Comparison of the oxygen reduction reaction on gold (red) and platinum (black) in ADW samples. CVs were performed from 1.2 V to −1 V for gold and −0.8 V for platinum. 1st and 2nd on the gold scan refers to each step in the two step oxygen reduction reaction. (b) Comparison of LSVs in 200 μmol hydrogen peroxide for gold (red) and platinum (black). LSVs were performed from −0.2 V to 0.8 V at 50 mV/s. INSET: Full calibration of hydrogen peroxide from 20 μmol to 1000 μmol (Platinum collector).

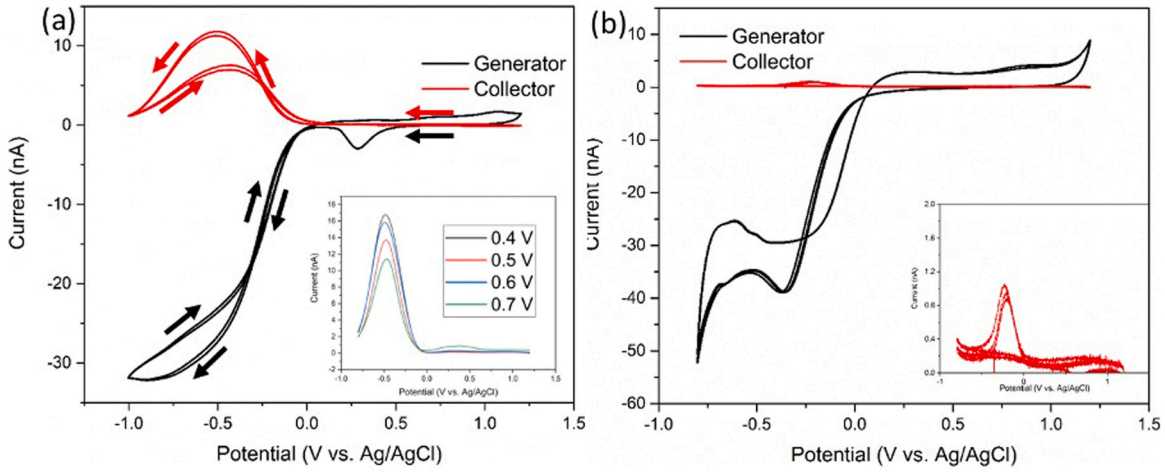

Fig. 3. (a) Gold-gold array in ADW showing oxygen reduction at the generator (black) and hydrogen peroxide oxidation at the collector (red). CV was performed from 1.2 V to −1 V at 50 mV/s with the collector biased at 0.4 V. INSET: The effect of varying the collector potential on the resultant scan, between 0.4 V and 0.7 V. (b) Equivalent scan to (a) performed on a platinum-platinum array. (Inset) shows a close-up of the collector scan highlighting the relative lack of hydrogen peroxide.

peroxide was produced on the reverse sweep, albeit lower than the forward sweep. Platinum, however, showed no hydrogen peroxide formation at all on the reverse sweep. This indicates that the presence of a surface platinum oxide in some way facilitates the production of hydrogen peroxide. The amount produced, however, was still too low for platinum to be considered a viable generator electrode for peroxide generation. Furthermore, there is no change to the platinum generator signal when the collector is appropriately biased, as no redox cycling occurs, highlighted in the supporting information (SI Fig. 5).

3.3. *Platinum plating on collector comb of an IDE array*

Based on these observations, it was postulated that a gold generator and a platinum collector would provide the optimum sensor performance. Therefore, platinum was electroplated onto one comb of a gold IDE to create a mixed gold-platinum IDE based sensor. This was

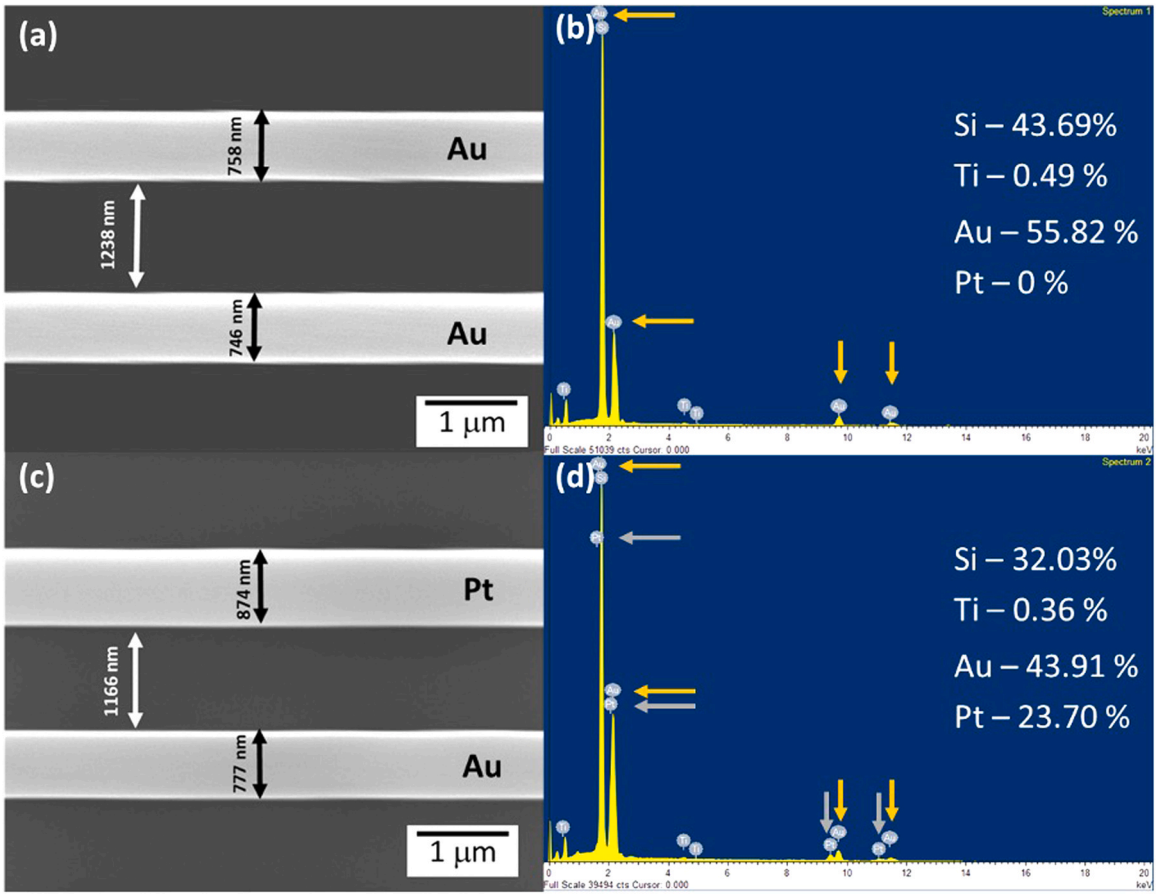

Fig. 4. (a) SEM of the gold-gold array prior to platinum plating. (b) EDX analysis of a gold-gold array, gold arrows indicate gold peaks. (c) SEM image of a gold-platinum array. (d) EDX analysis of a gold-platinum array, gold arrows indicate gold peaks, grey arrows indicate platinum peaks.

undertaken using a commercial platinum plating bath as described in the experimental section. The datasheet defined optimum parameters for plating were a current bias of 1 A/dm^2 of electrode surface to give a deposition rate of 5 μm/hr. As the surface area of one comb of electrodes was 1.08×10^{-7} dm^2, the applied current was set at 0.108 μA. It was found that the optimum deposition thickness was 100 nm for 60 s plating, at which complete coverage of the electrode was observed. Following the plating procedure, the electrodes were characterised to determine the platinum coverage using SEM and energy dispersive x-ray (EDX) spectroscopy. Both techniques were performed on the gold-gold and the gold-platinum IDEs for comparison. Fig. 4(a) shows the SEM and EDX, respectively, of a gold-gold IDE. From SEM analysis it was determined that both the generator and collector combs were approximately the same width (0.75 μm), and the gap was slightly over 1.24 μm. The electrodes shown in the SEM image were electrically independent of each other, such that plating on one of these electrodes should not impact the other electrode. EDX was performed on both electrode combs and spectra were obtained for each. The EDX spectra shown in Fig. 4(b) shows that gold was the dominant species present, indicated by the arrows. The SEM image in Fig. 4(c) for the platinum plated electrode indicates that approximately 100 nm of platinum was deposited on the collector comb of electrodes. The platinum comb width increased to 874 nm, and subsequently the gap decreased to 1.17 μm. The EDX spectrum for a plated electrode shown in Fig. 4(d) highlights that while gold was still the dominant species, platinum was also present on the surface, indicated by the silver-coloured arrows. The underlying gold was found to be dominant in the EDX spectrum since only a very thin layer of platinum was deposited. Thus, the X-rays can penetrate through the platinum layer and detect gold. The titanium adhesion layer beneath the gold, was also detected in trace amounts. An EDX was also performed on the unplated gold comb of electrodes. This was done as the width of the gold electrodes seemed larger than the non-plated IDE (777 nm vs. 758 nm). The EDX showed that no platinum was present on the gold electrode, and the larger width may have been due to variability in the fabrication process as it utilises optical lithography materials optimised for a 1.5 μm minimum feature fabrication process.

CV was then performed in single mode at the plated comb. Fig. 5(a) shows a comparison of CVs of 1 mM FCA at a gold comb before and after the comb had been plated with platinum. The observed peak shaped behaviour is again a result of diffusional overlap, which resulted in time dependent diffusion-limited mass transfer behaviour and a reduction peak for the oxidised FCA on the reverse sweep at approximately 0.22 V. The oxidation peak current at 0.35 V increased by approximately 1 nA as a result of the platinum plating, consistent with an increased surface area. A significant behaviour change was seen on the platinum coated electrodes, with a reduction current apparent between 0 V and 0.1 V. This was determined to be the onset of oxygen reduction. Again, this further indicated that platinum had deposited onto the electrode comb, as it reduces oxygen at more anodic potentials than gold. Typical deposition data is shown in the inset of Fig. 5(a).

The performance of the gold-platinum IDE was further tested by performing CVs in generator-collector mode using FCA as the redox molecule, wherein the platinum comb was kept as the collector electrode to determine if the platinum plating degraded the overall IDE performance. Fig. 5(b) shows a typical CV for FCA in generator-collector mode at either a gold-gold IDE or a gold-platinum IDE. In this case, the collector was biased at 0 V to reduce the oxidised species produced at the generator. The current has been amplified approximately 5 times with respect to the non-generator-collector mode scans and the CVs show excellent sigmoidal shape in keeping with diffusionally independent microelectrodes. A collection efficiency of 91.1 % was calculated from the limiting current of the generator and collector scans when both electrodes were gold, which was typical for the 1.2 μm gap IDEs. The same procedure was performed on the IDE where one comb had been plated with platinum. No significant changes were observed for this CV, with the gold electrode behaving as expected. This indicated that the platinum plating did not cause shorting between the generator and collector combs of electrodes. The current at the generator electrode remained the same, which is also expected as the surface area of the gold did not change. The current measured at the collector however, increased by 3 nA compared to the gold collector, arising from increased surface area of the platinum plated electrode. This increase also yielded an enhanced collection efficiency for the gold-platinum IDE of 95.7 %, an increase of 4.6 % over the gold-gold array. The increase in collection efficiency resulted from increasing the width of the electrode, which subsequently decreased the gap between the generator and the collector electrodes. As previously discussed, increased electrode width and decreased gap size are the main methods of enhancing the efficiency of diffusion-only generator-collector devices.

3.4. Generator-collector approach to DO quantification on gold-platinum arrays

Initial tests with platinum as a collector material indicated that the performance was worse than for bare gold. From the initial hydrogen peroxide experiments it was hypothesized that this should not be the case, as platinum outperformed gold. Analysis determined that the imposition of a constant bias at the platinum may cause the adsorption

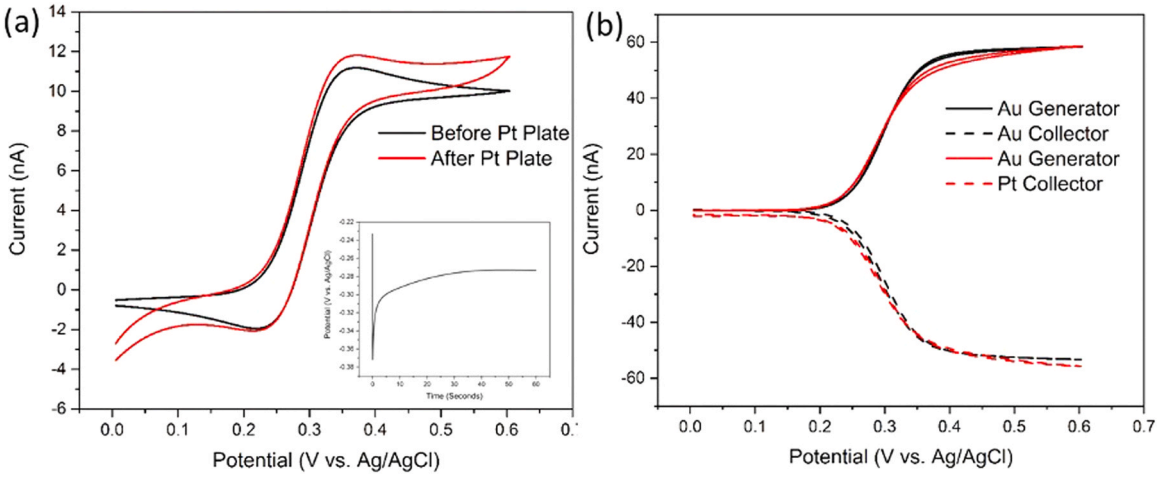

Fig. 5. (a) CVs on one comb of the interdigitated array in 1 mM FCA before (black) and after (red) platinum plating. CV's were performed from 0 V to 0.6 V at 50 mV/s. INSET: Typical chronamperogram recorded during the plating procedure. (b) CV's of a gold-gold array and a gold-platinum array in 1 mM FCA as before, with the addition of a collector electrode (dashed lines) biased at 0 V.

of oxygen species, which limits the performance of the collector electrode. To rectify the issues, a pre-treatment step was employed before any analysis was undertaken which involved biasing the platinum comb at −0.5 V for ten seconds prior to oxygen measurement. This removed any bound hydrogen peroxide, and had the benefit of reducing any surface oxide that may have formed during previous scans. A comparison of the collector data for untreated gold-gold and gold-platinum IDEs and a gold-platinum array that was pre-treated is shown in Fig. 6. Each of these scans had been performed in ADW with equivalent concentrations of DO. It is evident that the pre-treatment step is critical to ensure enhanced detection of hydrogen peroxide at the collector electrode. Having established the correct pre-treatment parameters, the effect of varying the collector potential was also investigated. From the initial work with hydrogen peroxide it was expected that a bias of 0.7 V would give the highest current, but ultimately it was determined that 0.4 V was more than sufficient, as shown in the inset of Fig. 3(a).

The gold-platinum arrays were subjected to varying concentrations of DO in ADW. Fig. 7(a) shows the generator CV result for the gold comb of electrodes, showing oxygen reduction at various DO concentrations. As with the initial tests on gold in generator-collector mode, the amplification of the hydrogen peroxide generation step results from redox cycling, particularly at high DO concentrations. The calibration plot of Fig. 7(a) is included in the supplementary information (SI Fig. 6), and exhibited a sensitivity of 4.11 nA/ppm, which is higher than those discussed previously for gold or platinum in single mode. This indicates that the redox cycling approach is more sensitive to DO, without yet taking advantage of the collector for interference elimination. Fig. 7(b) shows the resultant collector scans recorded on platinum (at 0.4 V) while the generator was undergoing CV. The oxidation reaction observed at −0.5 V is shown to scale with the DO concentration and occurs when the generator is reducing DO. The oxidation event observed at ~0.3 V seems to be in response to the gold oxide reduction occurring on the generator electrode which was only observed on the first CV sweep and not present in subsequent sweeps, which is shown in supporting information (SI Fig. 7 (a) and (b)). Fig. 7(c) shows that the current associated with the oxidation reaction at −0.5 V is linearly proportional to the amount of DO present in the solution, with a sensitivity of 1.49 nA/ppm. ($R^2 = 0.98$). The slight deviation from linearity in this data for DO concentrations around 4–4.5 ppm is likely due to the experimental set up. The samples were purged with nitrogen prior to measuring the oxygen concentration with an optical DO probe which required a volume of 50 mls for measurement. A portion of the 50 mls purged water sample was then transferred to the electrochemical cell (1 mL) and the different volumes measured could be responsible for the slight underestimation of the oxygen concentration measured. As described earlier in Section 2.5, the water samples dissolved oxygen rapidly between 0 and 4 ppm, and significantly more slowly for higher concentrations. Fully sealed or automated transfer of solution between the optical DO probe chamber and the microelectrode cell could further minimise any small concentration deviations. A limit of detection for this method of 0.36 ppm was calculated by using the formula 3.3σ/Slope, where the σ was calculated by 7 replicates of the 1 ppm sample.

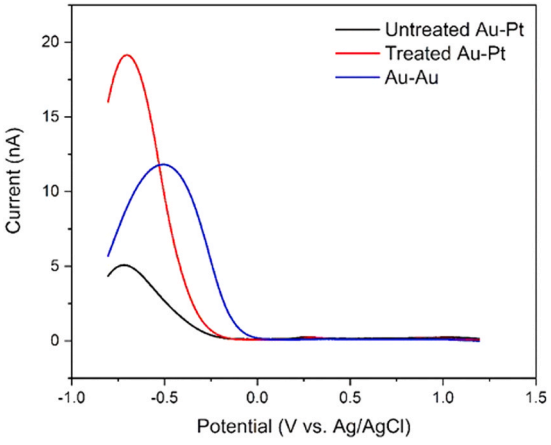

Fig. 6. Collector currents recorded for an imposed bias of 0.4 V while the generator was swept from 1.2 V to −0.8 V at 50 mV/s in 10 ppm ADW samples for untreated IDE arrays of gold-gold (blue) and gold-platinum (black) and a treated gold-platinum array (red).

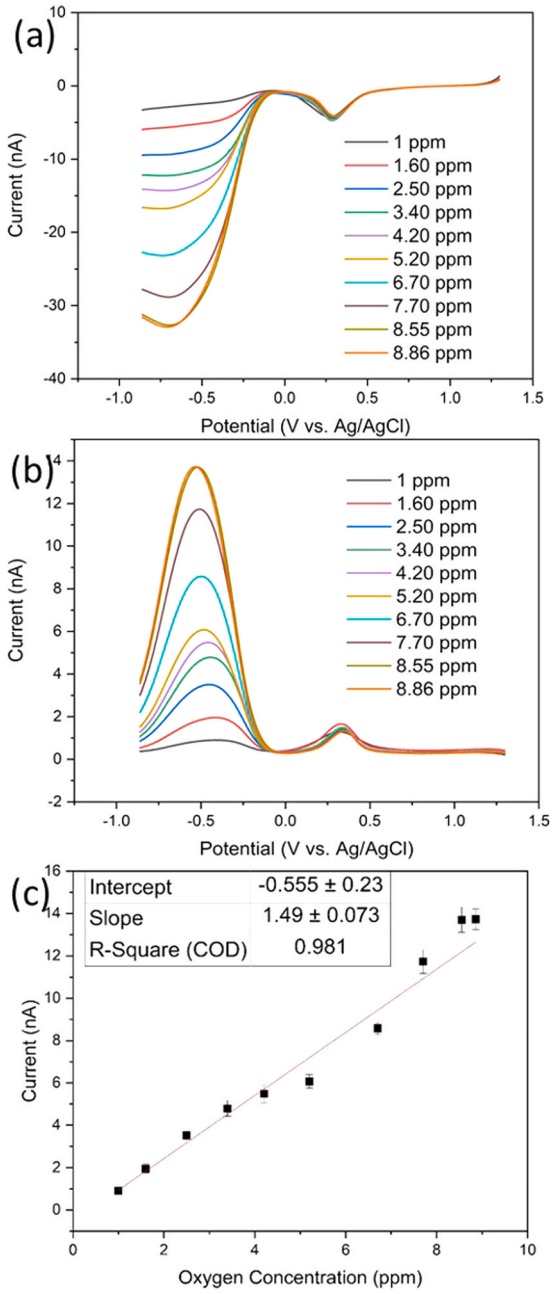

Fig. 7. (a) Gold generator electrode in various concentrations of DO in ADW. CVs were performed from 1.2 V to −0.8 V at 50 mV/s. Only the forward sweep of the CVs are shown for visual simplicity. The full CVs are included in SI-Fig. 8 (b) Platinum collector scans recorded while the generator was undergoing CV scans. The collector was held at 0.4 V in each scan. (c) Calibration plot for the collector currents measured as a function of DO concentration.

3.5. Effect of interferents on DO quantification via hydrogen peroxide oxidation

To assess interference effects, a sample of river water was collected and tested using the Au-Pt generator-collector method. River water was taken directly from the estuarine River Lee in Cork City at low tide, when the water was slow moving, in early May. Low tide was chosen for two main reasons:(i) contaminants present would likely exist in the greatest concentrations. (ii) DO concentration of running water is significantly higher than that of stagnant or slow-moving water. Fig. 8 shows voltammograms for equivalent tests performed in both ADW and the river water samples. In both samples, DO concentrations were ~ 4.5 ppm, confirmed by using the optical DO probe, with the ADW requiring a moderate purge to match the river water sample. The river water sample was equilibrated to room temperature before any measurement was taken. This likely would have changed the DO concentration, as water dissolves more oxygen at lower temperatures. However, as this test was only being done to compare the effectiveness of the method and not get representative data of actual water quality, this was not a concern for this approach at this time. The generator scans in Fig. 8(a), show a clear and significant increase in current is observed for the river water sample when compared to the ADW. This is attributed to other chemical interferent species being present in the water samples that may contribute to the increased reduction current and thus providing a false positive result. Fig. 8(b) shows the equivalent collector scans measured as the generator electrode was scanned. Very little deviation is observed for the current measured by comparison with the generator current. Using the calibration of the generator current described in the supporting information (SI Fig. 6) the difference in current at the generator electrode equates to a 3.4 ppm overestimation in the DO concentration. The collector signal, however, shows a 0.6 ppm underestimation of the DO concentration. Considering the difficulty associated with keeping samples at set DO concentrations, 0.6 ppm can be considered within experimental error.

Tests were performed with ADW samples that included known concentrations of reductive interferents. In this case, ADW samples were spiked with 1 ppm each of NaOCl and $FeCl_3$. Fig. 9 shows a bar chart of the resulting generator and collector signals. The blank measurement in ADW is considered 100 %. For this method, to account for the variability of DO, the signals were normalized based on their DO concentrations after they had been spiked with the interferent. In this process, samples were spiked with either NaOCl or $FeCl_3$ and equilibrated for 5 min before a DO measurement was taken with the commercial probe. The measured DO concentrations were then used to determine a ratio for the resulting measured signals. In both cases, the generator signal increases significantly upon addition of interferent, however, the collector signal remains relatively unchanged. This further indicates the effectiveness of the GC approach for the quantification of DO in water without the need for gas permeable membranes.

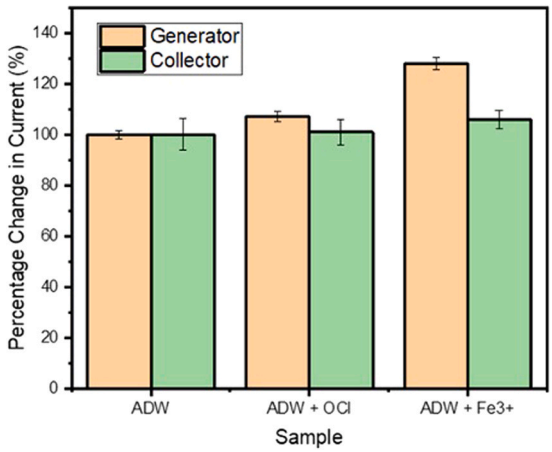

Fig. 9. Bar chart showing the effect of adding reductive interferents into an ADW sample. ADW is treated as the baseline, where deviations from 100 % indicate a current increase by said amount.

4. Conclusions

This work focused on the development of a membrane-free electrochemical based DO sensor using IDEs. It was determined that the ideal sensor for detection of DO should contain a gold generator electrode to produce hydrogen peroxide, and a platinum collector electrode to subsequently detect the hydrogen peroxide. To facilitate this, platinum was plated onto one comb of a gold interdigitated array. This had the additional benefit of decreasing the inter-electrode gap, thereby increasing the collection efficiency. The dual metal IDE was then used to calibrate DO in water using CV. A pre-treatment step was developed that improved the sensitivity of platinum to hydrogen peroxide by ensuring a clean, reproducible surface for each test. The developed sensor accurately detected oxygen concentrations between ~0 and 9 ppm, with a sensitivity of 1.59 nA/ppm and an LOD of 0.36 ppm. The detection of oxygen was also tested in the presence of unknown interferents, as in river water, and known interferents. It was found that the magnitude of hydrogen peroxide oxidation was generally unaffected by the presence

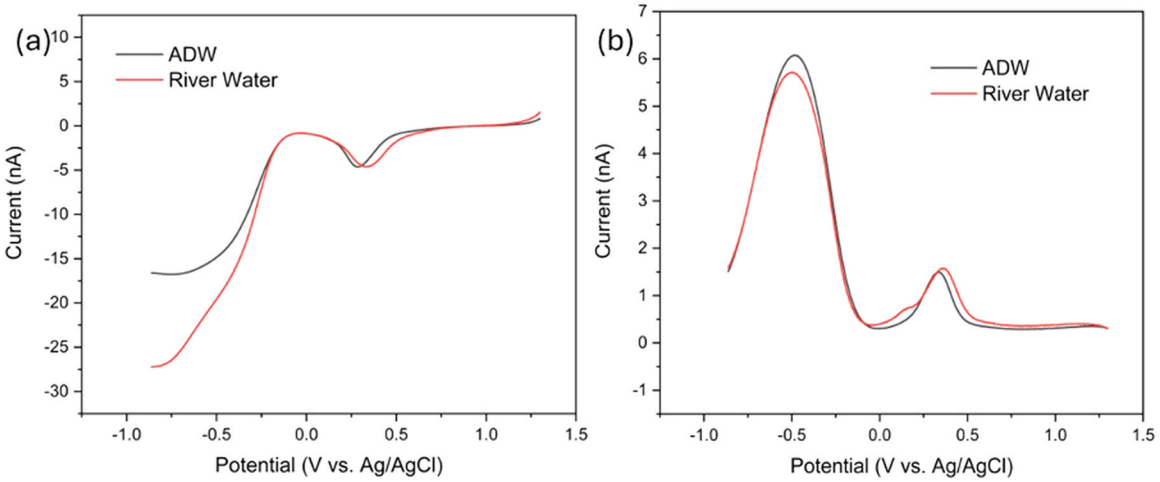

Fig. 8. (a) Gold generator electrodes in a river water sample (red) and an ADW sample (black) with equivalent concentrations of DO (5.2 ppm). (b) Resultant platinum collector scans obtained by biasing the collector at 0.4 V during the generator CV for river water (red) and ADW (black).

of interferents, indicating a potential for interferent free oxygen detection without the requirement of oxygen permeable membranes.

CRediT authorship contribution statement

James F. Rohan: Writing – review & editing, Supervision, Resources, Project administration, Methodology, Investigation, Funding acquisition, Conceptualization. **Alan O'Riordan:** Writing – review & editing, Supervision, Resources, Project administration, Methodology, Investigation, Funding acquisition, Conceptualization. **Fiona Barry:** Investigation, Formal analysis. **Ian Seymour:** Writing – original draft, Visualization, Validation, Investigation, Formal analysis, Data curation.

Declaration of Competing Interest

The authors declare that they have no known competing financial interests or personal relationships that could have appeared to influence the work reported in this paper.

Acknowledgements

This publication has emanated in part from research supported by a research grant from Science Foundation Ireland and the Department of Agriculture, Food and Marine on behalf of the Government of Ireland under the Grant 21/RC/10303_P2 (Vistamilk), and supported from research conducted with the financial support of Science Foundation Ireland (SFI) and is co-funded under the European Regional Development Fund under Grant Number 13/RC/2077_P2 (Connect) and under European Union's Horizon Europe research and innovation programme under the topic of ZEROPOLLUTION BioSensei Grant agreement ID: 101135241

Appendix A. Supporting information

Supplementary data associated with this article can be found in the online version at doi:10.1016/j.snb.2025.138689.

Data availability

Data will be made available on request.

References

[1] M. Mader, C. Schmidt, R. van Geldern, J.A.C. Barth, Dissolved oxygen in water and its stable isotope effects: a review, Chem. Geol. 473 (2017) 10–21, https://doi.org/10.1016/j.chemgeo.2017.10.003.
[2] R.J. Wilcock, G.B. McBride, J.W. Nagels, G.L. Northcott, Water quality in a polluted lowland stream with chronically depressed dissolved oxygen: causes and effects, N. Z. J. Mar. Freshw. Res. 29 (1995) 277–288.
[3] N. Zhao, Z. Fan, M. Zhao, A new approach for estimating dissolved oxygen based on a High-Accuracy surface modeling method, Sens. (Basel Switz.) 21 (2021), https://doi.org/10.3390/s21123954.
[4] Q. Wang, J.-M. Zhang, S. Li, Minireview: recent advances in the development of gaseous and dissolved oxygen sensors, Instrum. Sci. amp Technol. 47 (2018) 19–50, https://doi.org/10.1080/10739149.2018.1453835.
[5] Y.J. Lee, J.Y. Park, A highly miniaturized dissolved oxygen sensor using a nanoporous platinum electrode electroplated on silicon, J. Korean Phys. Soc. 58 (2011) 1505–1510, https://doi.org/10.3938/jkps.58.1505.
[6] I. Helm, L. Jalukse, I. Leito, A highly accurate method for determination of dissolved oxygen: gravimetric winkler method, Anal. Chim. Acta 741 (2012) 21–31, https://doi.org/10.1016/j.aca.2012.06.049.
[7] I. Seymour, B. O'Sullivan, P. Lovera, J.F. Rohan, A. O'Riordan, Removal of dissolved oxygen interference in the amperometric detection of monochloramine using a ph control method. 2019 IEEE SENSORS, 2019, pp. 1–4, https://doi.org/10.1109/SENSORS43011.2019.8956674.
[8] J. Park, J. Chang, M. Choi, J.J. Pak, D.-Y. Lee, Y.K. Pak, Microfabricated Clark-type sensor for measuring dissolved oxygen. 2007 IEEE Sensors, 2007, https://doi.org/10.1109/icsens.2007.4388677.
[9] Y. Wei, Y. Jiao, D. An, D. Li, W. Li, Q. Wei, Review of dissolved oxygen detection technology: from laboratory analysis to online intelligent detection, Sens. (Basel Switz.) 19 (2019) 3995, https://doi.org/10.3390/s19183995.
[10] L.S.S. Santos, R. Landers, Y. Gushikem, Application of manganese (II) phthalocyanine synthesized in situ in the SiO2/SnO2 mixed oxide matrix for determination of dissolved oxygen by electrochemical techniques, Talanta 85 (2011) 1213–1216, https://doi.org/10.1016/j.talanta.2011.06.003.
[11] S.M. Silva, L.F. Aguiar, R.M.S. Carvalho, A.A. Tanaka, F.S. Damos, R.C.S. Luz, A glassy carbon electrode modified with an iron N4-macrocycle and reduced graphene oxide for voltammetric sensing of dissolved oxygen, Microchim. Acta 183 (2016) 1251–1259, https://doi.org/10.1007/s00604-016-1750-6.
[12] Y.L. Zheng, D. Mei, Y.-X. Chen, S. Ye, The redox reaction of hydrogen peroxide at an Au(100) electrode: implications for oxygen reduction kinetics, Electrochem. Commun. 39 (2014) 19–21, https://doi.org/10.1016/j.elecom.2013.12.005.
[13] Y. Zheng, W. Chen, X.-Q. Zuo, J. Cai, Y.-X. Chen, The kinetics of the oxidation and reduction of HYDROGEN PEROXIDE at a pt electrode: a differential electrochemical mass spectrometric study, Electrochem. Commun. 73 (2016) 38–41, https://doi.org/10.1016/j.elecom.2016.10.012.
[14] U.A. Paulus, T.J. Schmidt, H.A. Gasteiger, R.J. Behm, Oxygen reduction on a high-surface area Pt/Vulcan carbon catalyst: a thin-film rotating ring-disk electrode study, J. Electroanal. Chem. 495 (2001) 134–145, https://doi.org/10.1016/s0022-0728(00)00407-1.
[15] A. Bonakdarpour, M. Lefevre, R. Yang, F. Jaouen, T. Dahn, J.-P. Dodelet, J.R. Dahn, Impact of loading in RRDE experiments on Fe–N–C catalysts: Two- or Four-Electron oxygen reduction? Electrochem. SolidState Lett. 11 (2008) B105, https://doi.org/10.1149/1.2904768.
[16] V. Stamenković, T.J. Schmidt, P.N. Ross, N.M. Marković, Surface composition effects in electrocatalysis: kinetics of oxygen reduction on Well-Defined Pt_3Ni and Pt_3Co alloy surfaces, J. Phys. Chem. B 106 (2002) 11970–11979, https://doi.org/10.1021/jp021182h.
[17] A.J.C. Wahl, I.P. Seymour, M. Moore, P. Lovera, A. O'Riordan, J.F. Rohan, Diffusion profile simulations and enhanced iron sensing in generator-collector mode at interdigitated nanowire electrode arrays, Electrochim. Acta 277 (2018) 235–243, https://doi.org/10.1016/j.electacta.2018.04.181.
[18] T.A. Postlethwaite, J.E. Hutchison, R. Murray, B. Fosset, C. Amatore, Interdigitated array electrode as an alternative to the rotated Ring−Disk electrode for determination of the reaction products of dioxygen reduction, Anal. Chem. 68 (1996) 2951–2958, https://doi.org/10.1021/ac960327b.
[19] I. Seymour, B. O'Sullivan, P. Lovera, J.F. Rohan, A. O'Riordan, Elimination of oxygen interference in the electrochemical detection of monochloramine, using in situ ph control at interdigitated electrodes, ACS Sens 6 (2021) 1030–1038, https://doi.org/10.1021/acssensors.0c02264.
[20] I. Seymour, B. O'Sullivan, P. Lovera, J.F. Rohan, A. O'Riordan, Electrochemical detection of free-chlorine in water samples facilitated by in-situ ph control using interdigitated microelectrodes, Sens Actuators B Chem. 325 (2020) 128774, https://doi.org/10.1016/J.SNB.2020.128774.
[21] N. Creedon, C. Robinson, E. Kennedy, A.O. Riordan, Agriculture 4.0: development of serological on-Farm immunosensor for animal health applications, in, IEEE Sens 2019 (2019) 1–4, https://doi.org/10.1109/SENSORS43011.2019.8956677.
[22] S. Barry, A. Pescaglini, A. Wahl, K. Dawson, A. O'Riordan, Reducing charging currents at nanowire sensors: simulation, fabrication and evaluation. 2019 IEEE SENSORS, 2019, pp. 1–4, https://doi.org/10.1109/SENSORS43011.2019.8956531.

Ian Seymour completed his PhD degree at Tyndall National Institute in Cork, Ireland in 2021. His research consists of developing electrochemical sensors using dual electrode set-up for environmental analysis applications.

Fiona Barry completed her PhD degree at Tyndall National Institute in Cork, Ireland in 2023. Her research consists of developing electrochemical sensors for environmental analysis applications.

Alan O'Riordan received his PhD in 2005, from University College Cork, Ireland. He is a senior research fellow at the Tyndall National Institute and the group head for Precision Electrochemical Nanosensors. His research focuses on using nanomaterials & nano-fabrication to develop smart sensor systems, based on Raman spectroscopy and nanoelectrochemistry.

James Rohan received his PhD from the University of Southampton, UK in 1994. He is a senior researcher at the Tyndall National Institute. His research focuses on device design, electrochemical materials processing and device fabrication and test for micro/nano-electronics, energy storage and sensor applications.